Iterative Coarse to Fine Approach to Interpret Magnetic Flux Leakage Measurements

Buddhi Wijerathna*, Sarath Kodagoda*, Jaime Valls Miro* and Gamini Dissanayake*
*Centre for Autonomous Systems
University of Technology Sydney, NSW 2007, Australia
Email: buddhi.s.wijerathna@student.uts.edu.au

***Abstract*—Magnetic Flux Leakage (MFL) is a commonly used technology for non destructive evaluation. In this study a coarse to fine approach is proposed to interpret MFL measurements. Defect profile inferred from a Gaussian Process model was used in a unconstrained non-linear optimiser to further improve the accuracy. This framework was tested on 100 year old $600mm$ diameter cast iron pipes. The ground truth extracted using a $3-D$ laser scanner showed a good agreement with the generated remaining wall thickness profile . With the reliable interpretations, this approach can be successfully used in the decision making of the asset maintenance process.**

I. Introduction

Non destructive evaluation (NDE) has been in interest of the researchers for decades. Mainly because of the growing industrial need for reliable asset maintenance techniques. With the advancement of technology, in-service inspection is getting popular, where the service is not disturbed due to the asset management tasks specially in petrochemical and water industries.

Commonly used technologies includes pulsed eddy currents(PEC), Remote field technology(RFT) , Magnetic flux leakage (MFL) and ultrasonics (UT). Out of these MFL is one of the mostly used technologies as an in-line tool as well as an external tool. In MFL the test substance is magnetised using a strong excitation magnetic field either using permanent magnets or electro magnets. When there is anomalies in the material, flux tend to create a leakage field in the close proximity of the anomaly. Appropriate sensors are used to measure these leakage fields and those signals are further processed to interpret defect information. The use of modern advanced signal processing and interpretation techniques results in accurate, fast and reliable outcomes. In particular, machine learning methods has been well investigated to solve inverse problem.

With the advancement of processing power, more powerful iterative numerical methods along with machine learning can be employed to solve these inverse problems. This study is focused on the inverse modelling of MFL signals by employing numerical iterative coarse to fine approach, on top of state of the art machine learning techniques.

An initial "coarse" solution is generated using a non parametric model. In order to learn a relationship between a labelled data set supervised learning is used. The kernel based methods such as Gaussian Processes (GP) [8] enables flexible modelling which is more suitable for practical applications. In this study GP is used for non-linear regression as described in [12]. Later the "coarse" solution from regression is used as the initial seed for the optimiser. This stage is essential due to the existence of non unique solutions which converges the optimiser in local minima. At each iteration simulated response for a given defect profile is compared against the original measurement and simplex algorithm is used to generate the next possible defect profile. This iterative solver eventually results in an improved defect profile compared to the regression result.

Having a validated simulation model is the key to this approach. We use an analytical model as well as en experimental set-up to validate the FEA simulation model. Infinitely long surface-breaking cracks was considered by Zatsepin and Shcherbinin [13] in their model where they approximate a strip dipole in terms of magnetic charges induced by the external magnetic field on the bounding surfaces of a crack. Shcherbinin and Pashagin [11] extended that by modelling defects with finite dimensions. The analytical solution derived in section II is also based on these literature.

The rest of the paper unfolds as follows. In Section II we discuss the analytical model used in the validation process. Section III describes the FEA simulation model used for data generation as well as for iterative optimisation. Generated data and machine learning process is briefly presented in section IV followed by the iterative refine process in section V. Results and discussions is presented after in section VII.

II. Magnetic Flux Leakage Analytical model

For the following derivation, it is assumed that a Dipolar magnetic charge (DMC) is developed on the defect faces intersecting the exciting magnetic field as a result of its interaction with the excitation field as described in [3] and [5]. Moreover, local variations in magnetisation and permeability were avoided by assuming high magnetic excitation, corresponding to the saturation region of the material.

Lets consider a cylindrical defect with its longitudinal axis (z-direction) perpendicular to the applied magnetic field (x-direction) , as schematically represented in Figure 1. The magnetic field lines diverge around the low permeability flaw, inducing a DMC on the walls of the cylinder. The surface of the test substance is defined by the xy plane at $z = 0$, with the top area of the cylindrical defect centre at $(0, 0, 0)$, and its bottom area centred at $(0, 0, -b_1)$, where b_1 is the depth of the defect. The MFL signal induced by the type of defect just described was sampled in the region $z > 0$.

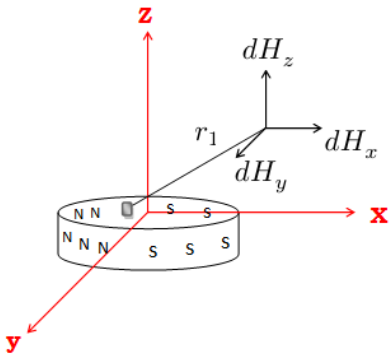

Fig. 1: Dipolar magnetic charge models for a cylindrical defect.

Half of the cylindrical defect develops a north polarity or positive magnetic charge density, $+\sigma$, while the other half has a south polarity or negative magnetic charge density,$-\sigma$. The cylindrical defect has a radius of R_1. The angle θ_1 is measured from the positive y direction to an element of magnetic charge, dp_1. The differential element of charge at the defect, dp_1, has coordinates $(R_1 sin\theta_1, R_1 cos\theta_1, z_1)$ and a charge proportional to its area. The magnetic field (dH_1) generated at a distance r_1 by this element of charge dp_1 is given by

$$dH_1 = \frac{dp}{4\pi r_1^3}.\mathbf{r_1} \tag{1}$$

Lets consider the positive polarity side H^+ of the defect and the axial component of the field at a distance r_{1+} are given by,

$$dH_x^+ = \frac{\sigma R_1 d\theta_1 dz_1}{4\pi r_1^3}\left(x + R_1 sin\theta_1\right) \tag{2}$$

Where,

$$r_1 = \sqrt{\left(x + R_i sin\theta_1\right)^2 + \left(R_i cos\theta_1\right)^2 + \left(h - z_1\right)^2} \tag{3}$$

Similarly the negative polarity side leakage field H^- of the defect is given by,

$$dH_x^- = -\frac{\sigma R_1 d\theta_1 dz_1}{4\pi r_1^3}\left(x - R_1 sin\theta_1\right) \tag{4}$$

The y component of the leakage field, dH_y^+, vanishes due to the symmetry. An integration of Equation 2 is applied over θ_1 from 0 to π and over z from $-b1$ $(b > 0)$ to 0 to determine the total field at r_{1+} due to the positively polarised side of the defect:

$$H_z^+ = \int_0^{\pi}\int_{-b1}^{0} \frac{\sigma R_1 (h - z_1)}{4\pi\left\{\left(x + R_i sin\theta_1\right)^2 + \left(R_i cos\theta_1\right)^2 + \left(h - z_1\right)^2\right\}^{\frac{3}{2}}} dz_1 d\theta_1 \tag{5}$$

By using the same integration for the negatively polarised side $H_z^-$of the cylinder the total normal leakage field along the $x = 0$ profile is given by,

$$dH_z = dH_z^+ + dH_z^- . \tag{6}$$

A. *Experimental comparison with analytical model*

The analytical model was implemented in MATLAB 8.2. Once it was implemented, the experimental signals was compared against the analytical model. Figure 5

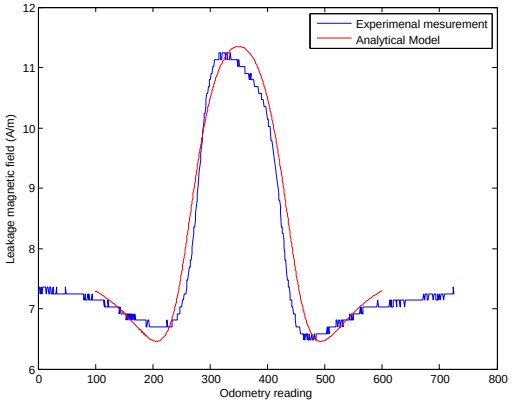

Fig. 2: Comparison of Analytical model and Experimental measurements

This analytical model does not consider the stray fields generated by the exciter coils which is present in a practical scenario. This field generates due to the flux that is not fully coupled into the test material. This is validated by having a constant non zero reading in the absence of a defect on the test material. This reading value was added to the analytical result to compare them against each other.

The analytical model is not applicable for complex defect shapes unless a approximation is used. Also this model does not take into account the non linear properties of the material. But the machine learning and optimisation process requires accurate MFL responses. Finite element analysis in computer based simulation software is designed to calculate very complex scenarios using numerical approaches. Although its computationally expensive, an FEA model was created for the purpose of accurate data generation. Section III describes the developed simulation model.

III. Simulation with Finite Element Analysis

As described above having a well calibrated simulation model is critical in this approach. Moreover the data set for

the supervised learning should cover most of the possible defect scenarios. It is also obvious that generating a dataset experimentally using the experimental set up is exhaustive and prohibitive. Therefore we employ a computer based simulation software to simulate the physical scenarios. Figure 3 shows the meshing of the FEA simulation model created using the AC/DC module of COMSOL Multiphysics software.

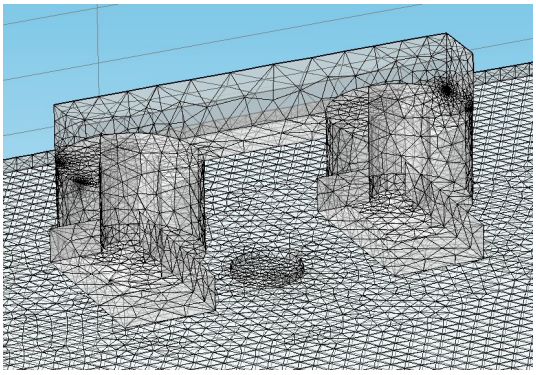

Fig. 3: Free tetrahedral mesh in FEA simulation

Two coils were applied in a U shaped yoke made of soft iron. These coils are used to excite the test substance by injecting magnetic flux. The measurements are taken $4mm$ above and parallel to the test plate. By defining a fixed sensor array, the repeatability of the simulated measurements is achieved. A very dense mesh, consisting 122686 elements was created in the simulation software which is shown in figure 3. The solution was extracted when the "relative tolerance" of each consecutive iteration goes below 0.1%. In order to validate the simulation model, a similar exercise was carried out in ANSYS software giving a 98.84% agreement in the signals. Figure 4 shows a comparison between the outputs of these two FEA packages.

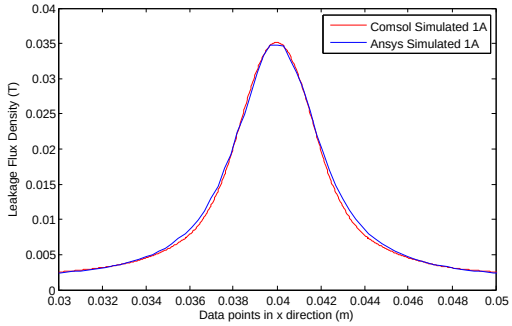

Fig. 4: Comparison of Ansys and Comsol Simulations

After development of the COMSOL simulation model, Analytical model was compared with that for verification purpose. As discussed above the analytical model does not account for the stray magnetic flux coming straight from the excitation coils. So a experimentally measured value of the stray field was embedded in the analytical model so that two curves can be compared with each other. See figure 5

Once the FEA model was validated, it was used to generate a data set covering a wide range of defects. These data was

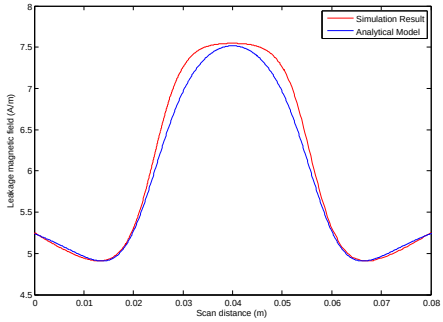

Fig. 5: Comparison of Analytical model and Comsol Simulations

then used as the training dataset for the GP learning process which is described in section IV

IV. Data interpretation with non-parametric models

In this section, we follow the framework introduced in "Multiple defect interpretation based on Gaussian processes for MFL technology" [12] . A non parametric model is developed using validated simulation data and applied to experimental measurements. This entire approach is illustrated in figure 6.

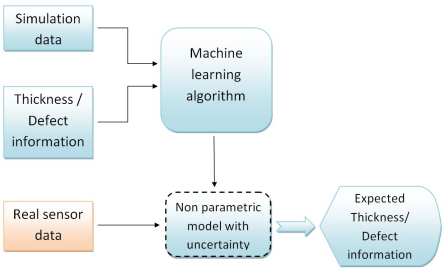

Fig. 6: Illustration of simulation based machine learning approach

Here FEA simulation data is used as the training data. Simulation data along with the thickness/defect information is used in a Gaussian processes [8] machine learning algorithm. Once the GP model learning process is completed, it is used to interpret defect information using real sensor data.

A. Gaussian processes modelling

Gaussian Processes (GP) are a non-parametric tool in the sense that they do not explicitly specify a functional model between inputs and outputs. GP can be thought of as a Gaussian prior over the function space mapping inputs and outputs [8].

The inverse problem inferring the defect profile using MFL signals is formulated as regression: estimating a function f mapping from inputs $\mathbf{u}$ to output $v = f(\mathbf{u})$. The hyperparameters, which is a part of the GP, needs to be learnt using realistic training data before using the model in regression.

The input to the learning algorithm is N noisy measurements $\mathbf{u}_{1,\ldots,N}$ associated with the outputs $v_{1,\ldots,N}$. Defining

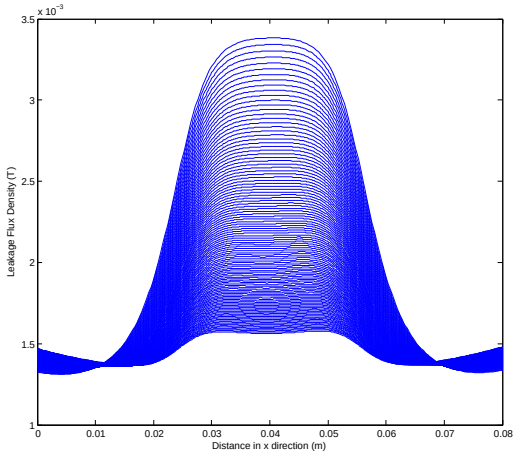

Fig. 7: Data generation for training

characteristic of a GP is that for any finite set of points $\mathbf{u}_{1,...,N}$, the marginal density $p(f(\mathbf{u}_1), f(\mathbf{u}_2), ..., f(\mathbf{u}_N))$ is a multivariate Gaussian. A Gaussian process is completely specified by its mean function $m(\mathbf{u}) = E[f(\mathbf{u})]$ and its covariance function $C(\mathbf{u}, \mathbf{u}^{'})) = E[(f(\mathbf{u}) - m(\mathbf{u}))(f(\mathbf{u}^{'}) - m(\mathbf{u}^{'}))]$ as $f(\mathbf{u}) \sim \mathcal{GP}(m(\mathbf{u}), C(\mathbf{u}, \mathbf{u}^{'}))$. The first step is to choose the form of $C(\mathbf{u}, \mathbf{u}^{'})$, which specifies the covariance of this Gaussian for any pair of points. The choice of covariance function is a form of model selection for automatic relevance determination, and should be consistent with prior knowledge about the type of function expected. We used the following covariance function for this study.

$$C(\mathbf{u}_m, \mathbf{u}_n) = C_i(\mathbf{u}_m, \mathbf{u}_n) + \sigma_v^2 \delta_{mn}, \tag{7}$$

where δ is the Dirac delta function and

$$C(\mathbf{u}_m, \mathbf{u}_n) = \sigma_f \exp\left(-\frac{1}{2}\sum_{l=1}^{L}\frac{\left(\mathbf{u}_m^{(l)} - \mathbf{u}_n^{(l)}\right)^2}{r^2}\right), \tag{8}$$

where $\beta = (\sigma_f, r, \sigma_v)'$ represent the hyperparameters of the covariance function. The second term in Equation 7 defines the sensor noise, σ_v^2 . Equation 8 encodes the correlations between measurements. $\mathbf{u}_n^{(d)}$ denotes the d_{th} component of $\mathbf{u}_n$, an d-dimensional vector, *i.e.* the dimension of the feature space.

Each observation y can be thought of as related to an underlying function $f(x)$ through a Gaussian noise model:

$$y = f(x) + \aleph\left(0, \sigma_n^2\right), \tag{9}$$

Regression is the search for $f(x)$. So, given v observations of y, our objective is to predict $\mathbf{y}_*$, which is given by,

$$\begin{bmatrix} y \\ \mathbf{y}_* \end{bmatrix} \sim \aleph\left(0, \begin{bmatrix} \mathbf{C} & \mathbf{C}_*^T \\ \mathbf{C}_* & \mathbf{C}_{**} \end{bmatrix}\right), \tag{10}$$

The conditional probability $p(\mathbf{y}_* \mid y)$: "Given the data, how likely is a certain prediction for $\mathbf{y}_*$? ", follows a Gaussian distribution. Our best estimate for $\mathbf{y}_*$ is the mean of this distribution.

$$\bar{y_*} = \mathbf{C}_* \mathbf{C}^{-1} y, \tag{11}$$

and the uncertainty in our estimate is captured in its variance:

$$var(y_*) = \mathbf{C}_{**} - \mathbf{C}_* \mathbf{C}^{-1} \mathbf{C}_*^T, \tag{12}$$

Next section talks about the training process carried out using above mentioned approach.

B. *Training the Models*

With the successful development of the simulation model of the tool, entire training was carried out using simulated data. During the training process the mode and the hyperparameters of the covariance function are learned. An example of the resulting variation of the features, namely the magnitude of the X component, with respect to the remaining wall thickness is illustrated in Figure 8.

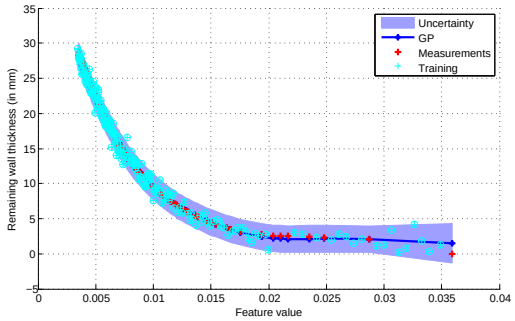

Fig. 8: Magnitude of the X component variation with the Remaining wall thickness

Once the model has been learned, it is used to infer the defect profile from fresh measurements[1]. Experimental measurements were taken on a aged water pipe in Sydney using the MFL lab set-up described in [12]. By extracting the ground truth forensically we could compare the interpretations against the ground truth. In order to achieve a more 'fine' defect profile, this inference result is fed in to a iterative optimiser which uses the simulation model generated in section III to generate the MFL response for each iteration.

V. Iterative Solver for the Defect Profile

In most of the cases the GP interpretation tends be more of a regional representation of the remaining wall thickness, rather than a point representation. This rises the need of a more detailed representation built on top of the GP interpretation. An iterative non-linear optimiser is used to address this problem. The estimated profile using the GP inference is used in the optimiser as the prior. Once the initial seed is given to the optimiser, it calls a FEA based Comsol simulator (as described in section III) to generate the MFL response. This response

[1]Note: In the validation process, we use a 3-fold cross-validation method

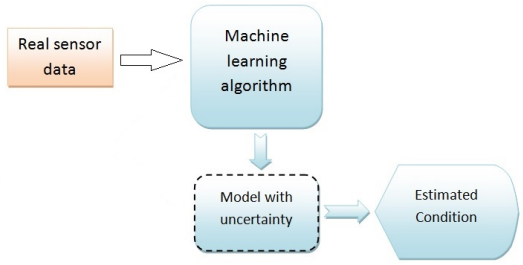

Fig. 9: Overview of the data interpretation approach

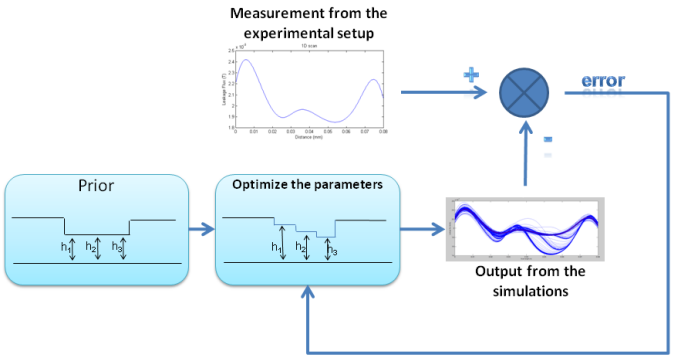

Fig. 10: Iterative solver for MFL signals

is then compared against the original measurement of the experimental set-up. By analysing the previous iterations and the current error, the simplex algorithm used in the solver generates a temporary defect profile, which again is fed into the simulator. Given the initial seed is a close solution, this iterative process converges to a near optimal solution giving a better 'fine' interpretation of the defect profile. This entire framework is shown in figure 10 .

VI. Results and Discussion

One of the main objectives of this research is to enhance the MFL interpretation using an iterative coarse to fine approach for cast iron water pipes. Water pipes exhumed from Sydney water test bed situated in Strathfield, Sydney was used for forensic analysis of the proposed method.

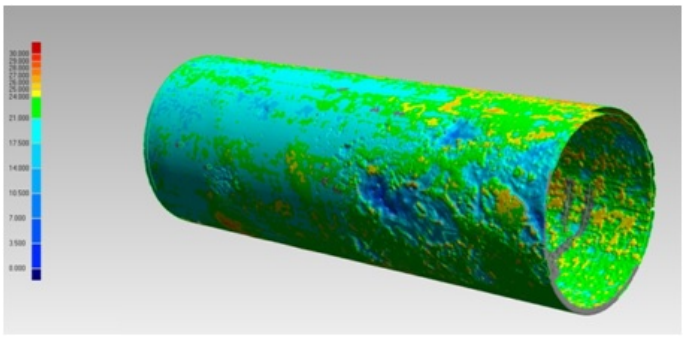

Fig. 11: 3-D model generated from the laser scanner

Once pipes were exhumed after 120 years of service, they were grit blasted to remove all non metallic substances. Then the pipes were scanned using the MFL lab set-up [12]. These data was used in the framework as testing data and interpretations were generated using GP inference. Later it was fed into the numerical optimiser. Its important to compare the interpretations with the ground truth to quantitatively evaluate the proposed method.

Fig. 12: 3-D laser scanner

It was rather a challenging process to extract the ground truth out of the grit blasted pipes. A $3D$ laser scanner 12 was used to scan the interested area and a 3D point cloud was generated. Later a ray tracing algorithm was employed to extract the ground truth. Figure 11 shows a $3D$ model of a pipe generated using the laser scanner.

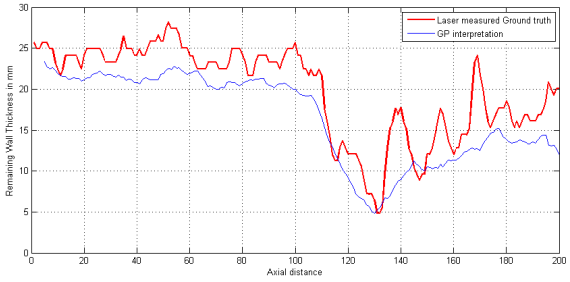

Fig. 13: GP Inference

First we use the experimental signal to generate the GP inference. This initial 'coarse' solution compared against the cross section of the ground truth is shown in figure 13. Starting from this seed iterative optimiser alters this profile to minimise the error between the measurement and the current MFL response. The numerical solver is set to terminate once the error margin drops below a certain level. Figure 14 shows the 'fine' result generated for the above example.

It is important to analyse the RMS error of the resulting cross section compared to ground truth and how it behaves with the number of iterations. Figure shows this analysis, the RMS error vs number of iterations. It is clear that with the number of iterations, the RMS error goes down, but eventually converges to a close to optimal solution.

As mentioned before, GP interpretation represents average RWT in a region rather than the point measurement which reduces the accuracy of the interpretation. But when its combined with this proposed iterative solver, it seems to find a solution close to the ground truth. Given the raster scan nature

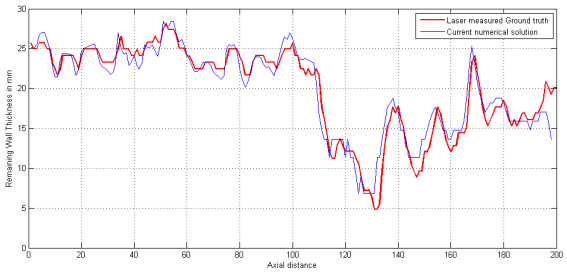

Fig. 14: Iterative 'fine' solution

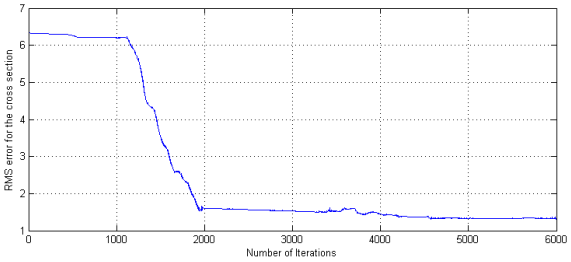

Fig. 15: RMS error variation with number of iterations

of MFL measurements, this method can be used to interpret an entire scan area in a higher resolution.

VII. Summary and Conclusions

In this study, we are presenting a coarse to fine approach to generate more realistic interpretations using MFL measurements.

A FEA based simulation model was developed to simulate the response of a experimental MFL set up. This model was validated using both analytical solution as well as experimental measurements. This FEA model is used to generate data with the required variety of defect scenarios to be used in the machine learning algorithm as well as in the refining process using an iterative solver.

The entire framework was tested using aged cast iron $600mm$ diameter water pipes exhumed from a Sydney Water Corporation test bed in Strathfield, Sydney. A $3D$ later scanner was used to extract the groundtruth from the grit blasted pipes. Interpreted profile was compared against the groundtruth giving a good agreement.

The main advantage of the entire framework is that it address the non unique nature of the MFL responses and also it achieves more accurate and detailed interpretations for MFL measurements.

In the current approach, although the sensor measurements are taken as a raster scan, only $1 - D$ samples of the signal is extracted for the entire process. In future we are planning to explore the usage of spacial features in the training process as well as in the optimisation process to take into account the spacial correlation between the defects.

Acknowledgements

This publication is an outcome from the Critical Pipes Project funded by Sydney Water Corporation, Water Research Foundation of the USA, Melbourne Water, Water Corporation (WA), UK Water Industry Research Ltd, South Australia Water Corporation, South East Water, Hunter Water Corporation, City West Water, Monash University, University of Technology Sydney and University of Newcastle. The research partners are Monash University (lead), University of Technology Sydney and University of Newcastle.

References

[1] A. Carvalho, J. Rebello, L. Sagrilo, C. Camerini, and I. Miranda, "MFL signals and artificial neural networks applied to detection and classification of pipe weld defects," *NDT & E International*, vol. 39, no. 8, pp. 661–667, Dec. 2006. [Online]. Available: http://linkinghub.elsevier.com/retrieve/pii/S096386950600034X

[2] S. Dutta, F. Ghorbel, and R. Stanley, "Dipole Modeling of Magnetic Flux Leakage," *IEEE Transactions on Magnetics*, vol. 45, no. 4, pp. 1959–1965, Apr. 2009. [Online]. Available: http://ieeexplore.ieee.org/lpdocs/epic03/wrapper.htm?arnumber=4802345

[3] C. Edwards and S. B. Palmer, "The magnetic leakage field of surface-breaking cracks," *Journal of Physics D: Applied Physics*, vol. 19, no. 4, p. 657, 1986. [Online]. Available: http://stacks.iop.org/0022-3727/19/i=4/a=018

[4] a. Khodayari Rostamabad, J. Reilly, N. Nikolova, J. Hare, and S. Pasha, "Machine Learning Techniques for the Analysis of Magnetic Flux Leakage Images in Pipeline Inspection," *IEEE Transactions on Magnetics*, vol. 45, no. 8, pp. 3073–3084, Aug. 2009. [Online]. Available: http://ieeexplore.ieee.org/lpdocs/epic03/wrapper.htm?arnumber=5170224

[5] C. Mandache and L. Clapham, "A model for magnetic flux leakage signal," *Journal of Physics D: Applied Physics*, vol. 36, pp. 2427–2431, 2003.

[6] K. Mandal and D. L. Atherton, "A study of magnetic flux-leakage signals," *Journal of Physics D: Applied Physics*, vol. 31, no. 22, p. 3211, 1998. [Online]. Available: http://stacks.iop.org/0022-3727/31/i=22/a=006

[7] J. V. Miro, J. Rajalingam, T. Vidal-Calleja, F. de Bruijn, R. Wood, D. Vitanage, N. Ulapane, B. Wijerathna, and D. Su, "A live test-bed for the advancement of condition assessment and failure prediction research on critical pipes," in *Proceedings of the Leading-Edge Strategic Asset Management Conference (LESAM13)*, 2013.

[8] C. Rasmussen and C. Williams, *Gaussian Process for Machine Learning*. Cambridge: MA:MIT press, 2006.

[9] M. Ravan, R. Amineh, S. Koziel, N. Nikolova, and J. Reilly, "Sizing of 3-d arbitrary defects using magnetic flux leakage measurements," *Magnetics, IEEE Transactions on*, vol. 46, no. 4, pp. 1024–1033, April 2010.

[10] R. Schifini and A. C. Bruno, "Experimental verification of a finite element model used in a magnetic flux leakage inverse problem," *Journal of Physics D: Applied Physics*, vol. 38, no. 12, p. 1875, 2005. [Online]. Available: http://stacks.iop.org/0022-3727/38/i=12/a=004

[11] V. E. Shcherbinin and A. I. Pashagin, "Influence of the extension of adefect on the magnitude of its magnetic field," *Defectoskopiya*, vol. 8, pp. 74–82, 1972.

[12] B. Wijerathna, T. Vidal-Calleja, S. Kodagoda, Q. Zhang, and J. Valls Miro, "Multiple defect interpretation based on gaussian processes for mfl technology," *Nondestructive Characterization for Composite Materials, Aerospace Engineering, Civil Infrastructure, and Homeland Security*, pp. 86 941Z–86 941Z–12, April 2013. [Online]. Available: + http://dx.doi.org/10.1117/12.2009966

[13] N. N. Zatsepin and V. E. Shcherbinin, "Calculation of the magnetostatic field of surface defects," *Defectoskopiya*, vol. 5, pp. 50–59, 1966.